A Knudsen Cell Study of the Heterogeneous Reactivity of Nitric Acid on Oxide and Mineral Dust Particles

G. M. Underwood,[†,§] P. Li,[†,§] H. Al-Abadleh,[†] and V. H. Grassian*[,†,‡,§]

Departments of Chemistry and Chemical and Biochemical Engineering and The Center for Global and Regional Environmental Research, University of Iowa, Iowa City, Iowa 52242

Received: June 21, 2000; In Final Form: April 18, 2001

The heterogeneous reactivity of gaseous nitric acid on α-Al_2O_3, α-Fe_2O_3, SiO_2, MgO, and CaO, as well as authentic samples of Gobi dust and Saharan sand, was investigated at 295 K using a Knudsen cell reactor. Through total uptake calculations and mass dependent studies, nitric-acid diffusion into the underlying layers is shown to be an important process for all of the systems studied. As such, models that account for the increased surface area and the concomitant increase in "internal collisions" were used to calculate uptake coefficients. The initial uptake coefficients for α-Al_2O_3, α-Fe_2O_3, SiO_2, MgO, and CaO all lie in the 10^{-5} to 10^{-3} region at gas concentrations between 10^{11} and 10^{12} molecules/cm^3. As expected, on the basis of their high SiO_2 composition, the measured initial uptake coefficients for the authentic dust samples are close to the value found for SiO_2 and are between 2 and 6×10^{-5}. Uptake of nitric acid on most of the oxide particles and the authentic dust samples results in irreversible adsorption. The effect of surface adsorbed water on both CaO and Gobi dust was investigated and is found to significantly enhance the initial uptake coefficient. Atmospheric implications of these results in terms of the importance of heterogeneous reactions of nitric acid on mineral aerosol are discussed.

Introduction

Although mineral aerosol is an important component of the earth−atmosphere system, little is known about its heterogeneous chemistry with atmospheric trace gases.[1] However, recent modeling results suggest that the reaction of mineral aerosol with nitric acid, in particular, may have a significant impact on the chemistry of the troposphere. For example, Dentener et al. studied the impact of irreversible reactions of HNO_3, N_2O_5, NO_3, HO_2, O_3, and SO_y on dust surfaces and determined that a large fraction of gas-phase nitric acid may be neutralized by mineral aerosol.[2] As a result, the regions where at least 40% of the total nitrate is found on the mineral aerosol covers vast areas of the Northern and Southern Hemispheres. During the months of February, March, and April, these regions cover almost all of Asia and extend throughout the central and northern regions of the Pacific Ocean basin and the tropical and sub-tropical Atlantic and Indian Oceans. Only the regions of Western and Central Europe, the eastern parts of North and Central America, and the high-latitude (>60°) zones are predicted to have relatively small portions of HNO_3 associated with the mineral aerosol. In addition, these effects can be intensified on regional scales during high dust periods, where surface areas of the mineral aerosol can be 1 order of magnitude higher than the monthly averaged values calculated by global models.[3,4] With emissions of mineral aerosol increasing as arid and semiarid areas expand due to shifting precipitation patterns and land use changes associated with overgrazing, erosion, land salinization, and mining/industrial activities,[5] it is essential to determine accurate heterogeneous uptake coefficients and rates for heterogeneous reactions.

In this regard, an understanding of the processes that control the concentration of nitrogen oxides is important to the development of models which can accurately describe tropospheric ozone and nitrogen-containing air pollutants.[6,7] As such, heterogeneous reactions that affect NO_x and HNO_3 concentrations have important implications for tropospheric chemistry. One problem encountered by present modeling efforts that rely on gas-phase chemical processes alone is that the calculated HNO_3-to-NO_x ratio is typically overpredicted by a factor of 5−10.[8−10] Heterogeneous processes that preferentially remove HNO_3 could potentially reconcile the predictions with the observations. In this study, we have investigated the heterogeneous uptake of nitric acid on oxide and mineral dust particles in order to assess its importance. In particular, the heterogeneous uptake of nitric acid on α-Al_2O_3, α-Fe_2O_3, SiO_2, MgO, CaO, and authentic samples of Gobi dust and Saharan sand was measured with a Knudsen cell reactor at 295 K under relatively dry conditions.

Several important conclusions come about from the study described here for the heterogeneous uptake of HNO_3 on oxide particles and mineral dust. It is shown that the pore diffusion model can be applied to HNO_3 reactions on oxide-powdered samples[11−14] and that the linear dependence of the observed uptake with oxide or dust sample mass, which we observed for NO_2 reactions,[15] is also apparent for the uptake of HNO_3 on relatively small amounts of powdered sample. These two approaches for taking into account gas diffusion into the powdered sample are quite good when the true uptake coefficient is less than 10^{-4} and saturation effects are minimal. For more reactive systems, saturation effects for each layer become important. Therefore, the Knudsen cell data are simulated using a kinetic model that takes into account gas diffusion into the

* Corresponding author.
† Department of Chemistry, University of Iowa.
‡ Department of Chemical and Biochemical Engineering, University of Iowa.
§ The Center for Global and Regional Environmental Research, University of Iowa.

10.1021/jp002223h CCC: $20.00
Published on Web 06/14/2001

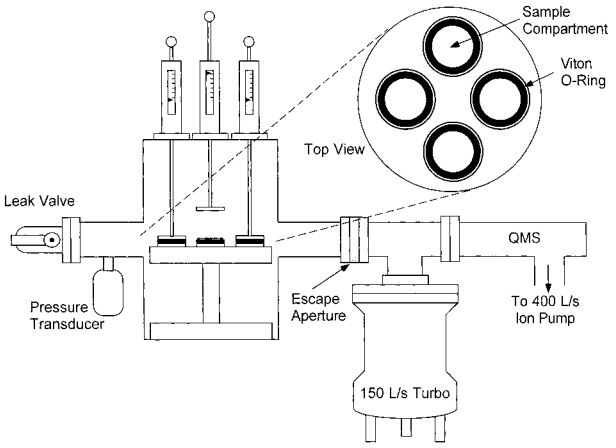

Figure 1. Schematic representation of the multisample Knudsen cell apparatus used in the experiments. All interior surfaces are coated with Teflon to provide a chemically inert surface.

underlying particle layers and saturation of the particle surface. The values of the initial uptake coefficient determined using the kinetic model are as much as a factor of 60 times higher in some cases than those determined from the simpler analysis using the linear mass dependence. We have also done a limited number of experiments to investigate the effect of adsorbed water and pressure on the heterogeneous uptake of HNO_3 on these particles. Finally, we discuss the atmospheric importance of nitric acid uptake on mineral aerosol using a recent box-model analysis.[16]

Experimental Section

Heterogeneous uptake coefficients were measured with a Knudsen cell reactor. A Knudsen cell reactor consists of a chamber with an isolated sample compartment and a small aperture or hole through which gas-phase reactant and product species can escape to be detected, usually by mass spectrometry. In a typical experiment, the sample compartment is covered while the walls of the reactor are passivated and a steady state flow is established. The pressure in the Knudsen reactor cell is kept low enough such that the mean free path of the molecules within the cell is greater than the cell dimensions so that boundary layer effects and homogeneous gas-phase collisions are minimized and can be neglected. The Knudsen cell reactor can be used at higher pressures, but to ensure molecular flow, the mean free path must be at least a factor of 10 greater than the diameter of the escape aperture.[17]

For the experiments described herein, a Knudsen cell reactor coupled to a UTI, DetecTorr II quadrupole mass spectrometer was used to determine uptake coefficients on powdered samples. Although the Knudsen cell reactor has been described previously,[15,18] it has recently been modified to allow for the analysis of multiple samples (Figure 1). A stainless steel reducing cross (6″−2.75″) now has four individual sample holders attached to a platform which rests on the bottom (6″) flange. All exposed interior surfaces are coated with Teflon to provide a chemically inert surface. Four Teflon-coated aluminum disks attached to four linear translators serve as covers for each of the powdered samples. The geometric area of each of the four sample holders is 5.07 cm^2. Since the volume of the sample holder is only about 2.5 cm^3 and the total volume is near 1500 cm^3, no corrections are needed to account for volume change upon opening the sample compartment. The seal between the sample holders and the cover is made with viton o-rings. With this setup, four samples of differing mass can now be analyzed in a single run.

TABLE 1: Sources of Samples and Tabulated Values of the Average Diameter and BET Surface Areas of Oxide Particles and Authentic Dust Samples Used in These Experiments

sample	source	average diameter (cm)	S_{BET} (cm^2/mg)
α-Al_2O_3	Aesar (#39814)	1.0×10^{-4}	140
α-Fe_2O_3	Aldrich (#31,0005-0)	6.9×10^{-5}	23
SiO_2	Degussa (Aerosil OX 50)	4.5×10^{-6}	500
MgO	Aesar (#14684)	2×10^{-5}	150
CaO	Aesar (#10923)	1.3×10^{-4}	39
Gobi dust	*a*	4.0×10^{-4}	110
Saharan sand	*b*	0.025	31

[a] China loess from the Gobi region (Nishikawa M., National Institute for Environmental Studies, Tsukuba, Ibaraki, Japan). [b] Galy-Lacaux C., Laboratory of Aerology, Observatory Midi-Pyrenes, Toulouse, France.

For each experiment, the nitric acid was allowed to flow through the reactor for at least 90 min prior to the experiment to passivate any possible wall reactions. The gas was introduced through a leak valve to the desired pressure as measured with an absolute pressure transducer (MKS 690A.1TRC range of 10^{-6} to 0.1 Torr). During passivation, the powdered samples were covered and sealed to avoid exposure to nitric acid. For the total uptake measurements, it was necessary to calibrate the flow out of the cell in terms of molecules per second. This was accomplished using the effective area of the escape aperture and the conversion of pressure to flux using the kinetic theory of gases. This gave the number of molecules per second escaping the cell as a function of pressure (i.e., molecules s^{-1} $\mu Torr^{-1}$). Multiplying this value by the experimentally determined absolute pressure versus the QMS intensity data (i.e., $\mu Torr\ A^{-1}$) yields a conversion factor through which the nitric acid mass spectrometer signal is converted to molecular flow through the cell. The nitric acid parent ion ($m/e = 63$) was monitored in these experiments. In addition to HNO_3, the mass spectrometer was also set to monitor other mass channels, including H_2O ($m/e = 18$), CO_2 ($m/e = 44$), NO ($m/e = 30$), NO_2 ($m/e = 46$), HONO ($m/e = 47$), and N_2O ($m/e = 44$). NO ($m/e = 30$) and NO_2 ($m/e = 46$) are also observed in the mass spectrum HNO_3, and the intensities of these two ions were found to follow the parent HNO_3 ($m/e = 63$) intensity.

It is very important that the powdered sample be evenly applied across the entire geometric area of the sample holder; otherwise, the measured initial uptake coefficient may reflect the amount of uncovered/unreactive surface in the sample holder as well as the sample mass. For preparing thin samples of the powdered samples, both of these concerns were addressed by using an atomizer to spray an aqueous slurry of the sample onto a heated sample holder. As determined with an optical microscope, this spraying procedure ensured very even coverage of the powdered sample across the bottom of the sample holder. Bulk density values were determined by weighing the amount of sprayed sample necessary to just fill a wide, shallow aluminum cup of known volume. Unless specifically stated otherwise, all powdered samples were placed in the Knudsen cell reactor and evacuated overnight prior to each experiment. All experiments reported here were done at $T = 295$ K.

The oxide-powdered samples used in these experiments were obtained from commercial sources. The source and relevant physical properties are given in Table 1. BET surface areas were measured using a multipoint BET analysis (Quantachrome Nova 1200). The chemical composition of the authentic dust samples determined by energy-dispersive X-ray analysis is given in Table 2. Dry gaseous nitric acid was taken from the vapor of a 1:3 by

TABLE 2: Chemical Composition in Atomic %[a], as Determined from Energy-Dispersive X-ray Analysis of the Saharan and Gobi Samples Used in These Experiments

element	Saharan sand	Gobi dust
Mg	0.49 ± 0.52	1.95 ± 0.99
Al	7.70 ± 2.08	10.11 ± 0.49
Si	81.40 ± 5.68	48.47 ± 5.64
K	1.76 ± 0.49	6.70 ± 1.04
Ca	1.29 ± 0.37	21.98 ± 6.80
Ti	0.54 ± 0.35	0.79 ± 0.50
Fe	6.83 ± 2.28	10.00 ± 1.20

[a] Excluding carbon and oxygen.

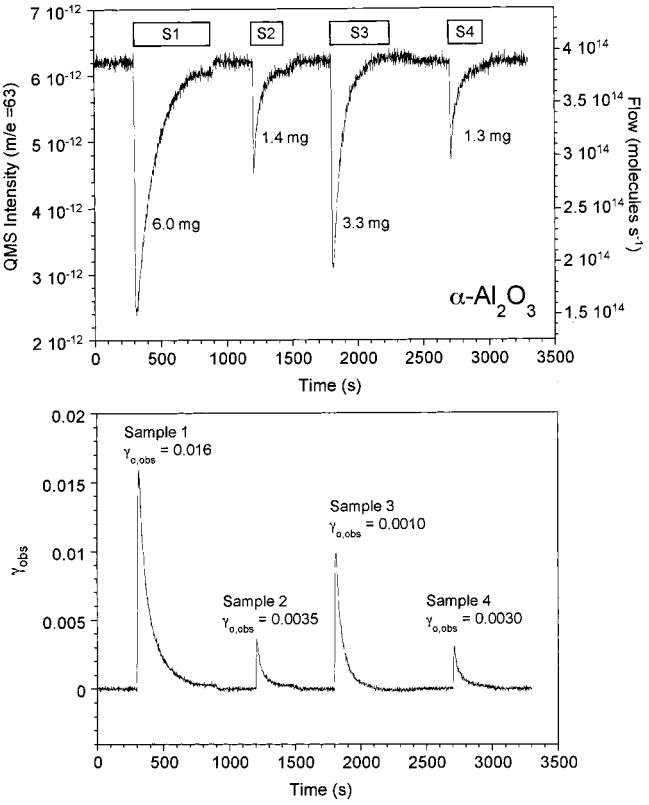

Figure 2. Upper panel: Typical Knudsen cell data for the uptake of nitric acid on four different samples (S1−S4) of α-Al_2O_3 represented in both QMS intensity ($m/e = 63$) (left axis) and flow (right axis). The rectangular boxes denote the times during which the sample compartments were opened. Lower panel: The uptake coefficients calculated for the data shown in the upper panel using eq 1 with an escape aperture of $A_h = 0.0484$ cm^2 and $A_s = 5.07$ cm^2. The initial pressure in the Knudsen cell was 40 μTorr (1.3×10^{12} molecules/cm^3). (Note that the escape aperture has been corrected for the Clausing factor,[21] i.e., $A_h = 0.150$ cm^2 $\times$ 0.320, where 0.320 is the Clausing factor. All of the escape apertures reported herein have been corrected).

volume mixture of concentrated HNO_3 (70.6% HNO_3, Mallinckrodt) and H_2SO_4 (95.9%, H_2SO_4, Mallinckrodt), which was purified by four freeze−pump−thaw cycles.

Results

Representative Knudsen Cell Reactor Data—Heterogeneous Uptake of HNO_3 on Oxide and Mineral Dust Particles. Typical Knudsen cell reactor data for the uptake of nitric acid on varying amounts of α-Al_2O_3, SiO_2, and Gobi dust are shown in the upper panel of Figures 2, 3, and 4, respectively. The rectangles labeled S1, S2, S3, and S4 denote the times during which the lids for each of the four different samples were open and each of the four samples was exposed to gaseous nitric acid. The data are shown in terms of both QMS intensity of the

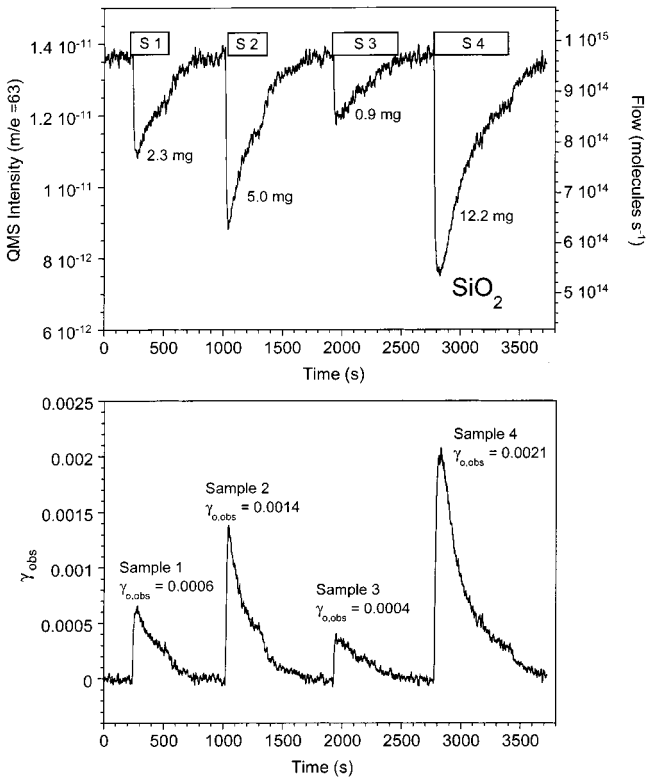

Figure 3. Upper panel: Typical Knudsen cell data for the uptake of nitric acid on four different samples (S1−S4) of SiO_2 represented in both QMS intensity ($m/e = 63$) (left axis) and flow (right axis). The rectangular boxes denote the times during which the sample compartments were opened. Lower panel: The uptake coefficients calculated for the data shown in the upper panel using eq 1 with $A_h = 0.0130$ cm^2 and $A_s = 5.07$ cm^2. The initial pressure in the Knudsen cell was 8 μTorr (2.6×10^{11} molecules/cm^3).

parent ion ($m/e = 63$) for nitric acid (left y-axis) and molecular flow (right y-axis). The conversion from QMS intensity to molecular flow is described in the Experimental Section.

The observed heterogeneous uptake coefficients determined for nitric acid on varying amounts of α-Al_2O_3, SiO_2, and Gobi dust were calculated using the Knudsen cell equation derived for steady-state uptake[17,19,20]

$$\gamma = \frac{A_{h,eff}}{A_s}\left(\frac{I_o - I}{I}\right) = \gamma_{obs} \qquad (1)$$

where $A_{h,eff}$ is the effective area of the escape hole or aperture accounting for the Clausing factor,[21] A_s is the geometric area of the sample holder, and I_o and I are the mass spectral intensities measured with the sample covered and exposed, respectively. The uptake coefficient calculated using eq 1 will be referred to as the observed uptake coefficient, γ_{obs}. As can be seen from the lower panels of Figures 2−4, the observed uptake coefficient, γ_{obs}, decreases with continued exposure. The observed uptake coefficient decreases to zero as the surface becomes saturated. As such, the values of the uptake coefficient reported here are the initial uptake coefficients and are taken as the maximum value of the uptake coefficient, $\gamma_{max,obs}$. From the lower panels of Figures 2−4, it can be clearly seen that the value of $\gamma_{max,obs}$ depends on the samples mass and thus the thickness of the sample and the number of layers of particles present in the sample.

The Knudsen cell equation given in eq 1 does not account for the observed mass-dependent behavior. This is because in deriving eq 1, the total number of gas surface collisions is taken

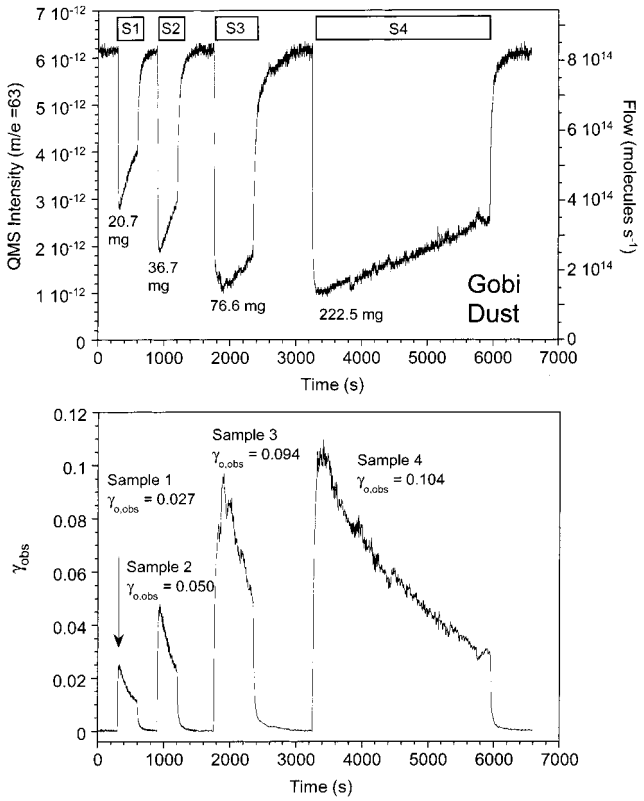

Figure 4. Upper panel: Typical Knudsen cell data for the uptake of nitric acid on four different samples (S1−S4) of Gobi dust represented in both QMS intensity ($m/e = 63$) (left axis) and flow (right axis). The rectangular boxes denote the times during which the sample compartments were opened. Lower panel: The uptake coefficients calculated for the data shown in the upper panel using eq 1 with $A_h = 0.104$ cm^2 and $A_s = 5.07$ cm^2. The initial pressure in the Knudsen cell was 40 μTorr (1.3×10^{12} molecules/cm^3).

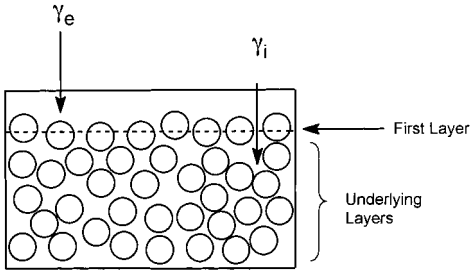

Figure 5. Graphical representation of a powdered sample in the sample compartment. External and internal contributions to γ_{obs} are indicated by γ_e and γ_i, respectively.

as the flux of molecules to the geometric area of the sample holder. Thus, it is assumed that each time a molecule approaches the sample, it collides only once and only with the top layer. If the sample were a liquid or a single crystal, this assumption probably would not introduce any substantial error. However for porous samples, the assumptions of a single collision on the top layer appears to be a simplification not warranted in these experiments. Gas diffusion models that take into account surface area are discussed below.

Pore Diffusion Model Adapted for Atmospherically Relevant Systems. In 1991, Keyser, Moore, and Leu adapted a model from the heterogeneous catalysis literature[14] to explain heterogeneous reactions of atmospheric relevance.[13] The model takes into account gas diffusion into the underlying layers of a porous sample by considering the contributions from both external (first layer) and internal (underlying layers) particle surface area (see Figure 5) in determining uptake coefficients. As the earlier work includes a complete set of justifications and derivations[13,14] that has been summarized in other publications,[11,12,15,18] the details will not be presented here. The premise of the model is that the true uptake coefficient, γ_t, can be thought of in terms of external and internal components which are related to the observed uptake coefficient, γ_{obs} by the following equation:[22]

$$\gamma_{obs} = \gamma_t\left(\frac{S_e + \eta S_i}{A_s}\right) \tag{2}$$

where

$$\eta = \frac{1}{\phi}\tanh(\phi)$$

and

$$\phi = \frac{m}{\rho_b A_s d}\left(\frac{3\rho_b}{\rho_t - \rho_b}\right)\left(\frac{3\tau\gamma_t}{4}\right)^{1/2}$$

The parenthetic term in eq 2 is a correction factor for the effect of gas-phase diffusion into the underlying layers. S_e and S_i are the external and internal surface areas, A_s is the geometric area of the sample holder, and η is a calculated "effectiveness factor". The effectiveness factor is the fraction of the internal area that contributes to the measured value of the uptake coefficient. Its value is mass (sample thickness) dependent and is determined from the relative rates of surface adsorption and diffusion into the underlying layers. Because of inhomogenieties in the interparticle voids, however, the effective diffusion constant is less than would be calculated assuming diffusion through long straight capillaries. This effect is accounted for by incorporating a tortuosity factor, τ. Models of porous solids have predicted τ values in the range of 1−8;[12−15] however, most porous solids, especially powders, are not characterized well enough for an accurate calculation of τ to be made, and thus, τ must be experimentally determined. The mass, m, the bulk density of the powder, ρ_b, the true density of the material, ρ_t, and the diameter of the particle, d, also enter into the calculation of η.

The form of the equation used in this paper is somewhat modified from the forms of earlier papers[11,13] in that here we did not assume either simple cubic or hexagonal close-packing spheres. Instead, the experimentally measured bulk density was used in the calculations. In addition, the specific BET surface area was measured rather than calculated. Rewriting eq 2 in terms of measured bulk density and BET surface area yields

$$\gamma_{obs} = \gamma_t \rho_b S_{BET}(h_e + \eta h_i) \tag{3}$$

where S_{BET} is the BET specific surface area, h_e is the height of the first layer, and h_i is the height of all the internal layers.

Application of the Pore Diffusion Model to the Heterogeneous Uptake of HNO_3 on MgO. Figure 6 depicts Knudsen cell data for the reaction of HNO_3 ($m/e = 63$) on MgO with different masses. These data are the result of several experiments for which the QMS intensity curves are over layed on top of one another. Again it can be seen, as with the previous examples, that the QMS signal is mass dependent and thus dependence on the number of layers of particles present in the sample. The total area of under the curve increases with sample mass as there are more surface sites available for adsorption for the larger samples.

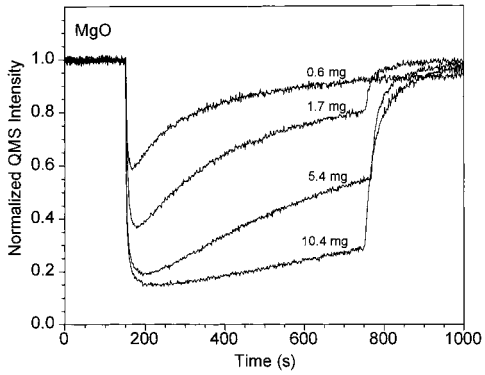

Figure 6. Knudsen cell data showing QMS intensity ($m/e = 63$) as a function of time in seconds for HNO_3 uptake on (in ascending order on the graph**)** 0.6, 1.7, 5.4, and 10.4 mg of MgO. The sample compartment was opened, for each mass, at 150 s. The sample compartment was closed at 750 s for all but the 0.6 mg experiment, which was closed at 1100 s. The following experimental parameters were used in these experiments: $A_h = 0.0484$ cm^2, $A_s = 5.07$ cm^2, and an initial pressure of 40 μTorr (1.3×10^{12} molecules/cm^3).

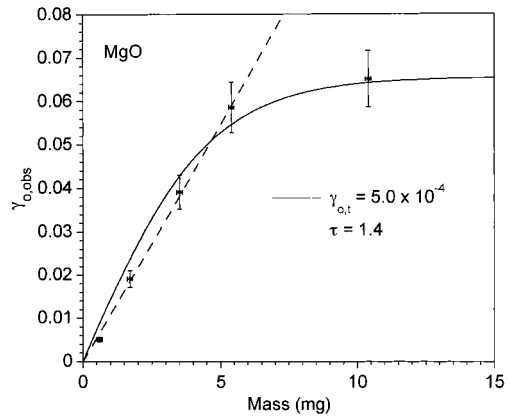

Figure 7. Initial uptake coefficients for HNO_3 on MgO taken from the data in Figure 6. The data points (filled circles) were calculated using eq 1. The X and Y error bars represent the mass resolution of ± 0.05 mg and experimental reproducibility of $\pm 10\%$ respectively. The solid lines are the results of the KML model using eq 3 and the parameters given in Table 3. The dashed line through the first four data points are a linear fit of the form $y = 0.01094x$, with $R = 0.99915$. Using this slope along with eq 5 and the data provide in Table 1, we determined the initial uptake coefficient to be 3.7×10^{-4}. This value is within 25% of the value determined using the KML model.

As discussed for α-Al_2O_3, SiO_2, and the Gobi Desert, if only the geometric area of the sample holder or, equivalently, if only the top layer of the powdered sample were contributing to the observed uptake coefficient, then there would be no mass dependence. The observed mass dependence indicates that diffusion into the underlying layers, with a concomitant increase in the number of collisions, is contributing to the observed uptake coefficient. To apply the pore diffusion model, it is necessary to fit the experimental data with two independent fitting parameters, namely, the true uptake coefficient,γ_t, and the tortuosity, τ.

As mentioned above, the experimental variable in the pore diffusional model for particles of a given size is the sample mass (sample thickness). The observed maximum uptake coefficient for HNO_3 on MgO as a function of sample mass is presented in Figure 7. An additional data point collected for 3.6 mg is included in this plot. The y error bars are $\pm 10\%$, based on experimental reproducibility (propagation of error yields a standard deviation of $\sim 5\%$), and the x error represents the precision of our mass balance, ± 0.05 mg. The best-fit result

TABLE 3: Equations and Physical Parameters Used in the KML Model for MgO[a–c]

parameter	symbol	MgO
diameter	d	2×10^{-5} cm
specific surface area	S_{BET}	150 cm^2 mg^{-1}
true density	ρ_t	3.58 g cm^{-3}
bulk density[a]	ρ_b	0.60 g cm^{-3}
true initial uptake coeff[b]	$\gamma_{o,t}$	5.0×10^{-4}
tortuosity[c]	τ	1.4

[a] Determined from a weight of known volume. [b] Best-fit values. [c] Other parameters calculated as follows: $h_e = 0.5$(particle mass/ρ_b)$^{1/3}$ = $^1/_2$ the height of one layer, and $h_{total} = m/(A_s\rho_b)$: $h_i = h_{total} - h_e$.

of the diffusion model for the HNO_3 uptake on MgO is shown as the solid line using $\tau = 1.4$ and $\gamma_t = 5.0 \times 10^{-4}$. The physical parameters and equations used in the model are given in Table 3. It can be seen that the model fits both the form and the absolute measured values exceptionally well. It should be noted that although there are two independent variables in the model, there are also two distinctly different regions of the data that need to be fit, the strongly mass-dependent (low mass) region and the plateau (high mass) region. As such, there is only a small range of γ_t and τ values that will fit the entire data set.

It should also be noted that for the heterogeneous uptake of HNO_3 on MgO, the mass dependence is only seen for very thin samples of mass less than 5 mg over an area of ~ 5 cm^2. Although experiments performed using a greater amount of sample will not show a mass dependence, this does not mean that the geometric area of the sample is the correct area use when calculating the true uptake coefficient. It means that only the plateau region is being accessed and thus all that can be said of the correct area to use is that it lies somewhere between the BET area of the entire sample and that of the first layer.

The example above demonstrates that it is possible for the pore-diffusion model to reproduce experimental results quite well. However the use of a calculated tortuosity, τ, as a fitting parameter is a major weakness of the analysis which is likely to invoke a certain amount of skepticism as to the accuracy of the resultant γ_t values, especially when the corrections used are very large. It should be noted that if the effective diffusion constant, D_{eff}, could be measured, the tortuosity factor would not be needed, and the only fitting parameter would be γ_t. This would enable the model to fit the plateau region uniquely with γ_t, eliminating the need to collect data in the linear region. Unfortunately, measuring D_{eff} for reactive gases within powdered samples is not an easy task, and there are very few reported values for relevant gas/powdered samples in the literature. As such, in the next section, a simple method that eliminates the need to know the effective diffusion constant and/or tortuosity factor is utilized.

Linear Mass-Dependent Regime. It can be seen from Figure 7 that there is initially a strong mass dependence and that as the sample mass increases the observed uptake value reaches a constant value. This trend of strong mass dependence for low-mass (thin) samples and no mass dependence for higher-mass (thicker) samples has been observed for reaction of NO_2 on oxide and mineral dust samples.[15,16] This observation is consistent with a "probe depth" below which essentially the entire sample is interrogated and, thus, has a linear mass dependence (LMD), above which the sample mass (depth) is unimportant. The extent of the probe depth depends on many factors, including γ_t, particle size, particle roughness, and the surface saturation coverage. As can be seen from Figure 7, the probe depth is very small for the MgO particles, as they are relatively small particles with high surface area. So long as it

is possible to make samples that are thin enough to be in the linear regime, LMD experiments are feasible.

For sufficiently thin powdered samples, the observed initial uptake coefficient, $\gamma_{o,obs}$ is directly proportional to the sample mass, and the entire sample is available to the reactant gas. This is termed the linear mass-dependent regime. Gas molecule diffusion beyond the first layer is not surprising when the arrangement of the particles is considered. The pore ratio, *X*, is the fraction of the first layer of particles that is open to the layers below; it is equal to 9.3% for hexagonal close-packed particles and 21.5% for cubic close-packed particles (assuming spherical particles). Frequently, especially for very small particles, neither close-packed arrangement is achieved, and the surface pore ratio is even higher. Thus, it is not surprising that diffusion into the underlying layers is a facile and significant process. The net effect is that molecules that approach the surface are likely to enter the underlying layers, where they will make many collisions with the sample before they are adsorbed or exit the sample. These extra collisions will significantly amplify the observed uptake coefficient.[15] The LMD model, then, can be used to determine the correction factor needed to account for the collisions that occur in the underlying layers. Though the derivation is somewhat involved, it leads to a very simple modification to the standard Knudsen cell equation in which the geometric area of the sample holder is simply replaced by the BET area of the sample

$$\gamma_t = \frac{A_{h,eff}}{A_{BET}}\left(\frac{I_o - I}{I}\right) = \left(\frac{A_s}{A_{BET}}\right)\gamma_{obs} \qquad (4)$$

where γ_t is the true uptake coefficient, A_{BET} is the BET area of the entire sample (i.e., the specific surface area times the sample mass), and all other variables are as described above. Equation 4 gives a simple correction factor with which the true uptake coefficient, corrected for multiple collisions with the entire BET sample area, can be extracted from the observed value, which assumes no diffusion into the underlying layers.

Further evidence that for sufficiently thin samples, the entire sample is interrogated during an experiment comes from quantitative measurements of the total uptake. This can be accomplished by calibrating the Knudsen cell for flow, in molecules per second, and then offsetting the raw data by the steady-state value and inverting it. In this manner the total integrated area is equal to the total number of molecules adsorbed on the surface. The surface coverage can then be calculated using the BET surface area. Typical data for an α-Al_2O_3 sample are presented in Figures 8. From simple geometric arguments, the maximum surface coverage, N_{max}, for nitric acid on these surfaces should be near $\sim 2 \times 10^{14}$ molecules cm^{-2}. The maximum surface area measured for α-Al_2O_3 at a pressure of 40 μTorr is 3.5×10^{13}.

Surface saturation coverages calculated for these samples are presented in Table 4. For CaO and MgO, it has been determined from separate experiments that reaction into the bulk of the these particles can occur; thus, the reaction is not limited to the particle surface,[23] and saturation coverages greater than 2×10^{14} molecules cm^{-2} are observed.

Applications of the LMD Model to the Heterogeneous Uptake of HNO_3 on Oxide and Mineral Dust Particles. The linear mass-dependent regions of the observed initial uptake coefficients for HNO_3 on α-Al_2O_3, α-Fe_2O_3, SiO_2, MgO, CaO, and authentic Gobi dust and Saharan sand samples are presented in Figures 7 and 9. In each case, the observed initial uptake coefficients, using the geometric area, are plotted along with a linear least-squares fit to the data of the form $Y = mX$ so that the fit is forced through the origin. The resultant correlation coefficients are greater than 0.99 for all samples except for Saharan sand. Efforts were made to precisely replicate experimental conditions such as pump down time, background levels, and operating pressure for each experiment; thus, the increased scatter for the Saharan samples is potentially due to differences in particle size distribution.

TABLE 4: Surface Saturation Coverages Determined from Calibrated Knudsen Cell Experiments

sample	coverage[a] (molecules cm^{-2})	concentration (μTorr)	concentration (molecules cm^{-3})
α-Al_2O_3	$3.5(\pm 0.7) \times 10^{13}$	40	1.3×10^{12}
SiO_2	$2.3(\pm 0.5) \times 10^{13}$	8	2.6×10^{11}
MgO	$7.0(\pm 1.4) \times 10^{14}$	40	1.3×10^{12}
α-Fe_2O_3	$6.9(\pm 1.4) \times 10^{13}$	10	3.3×10^{11}
CaO	$6.5(\pm 1.3) \times 10^{14}$	40	1.3×10^{12}
Gobi dust	$1.0(\pm 0.2) \times 10^{14}$	50	1.6×10^{12}
Saharan sand	$4.8(\pm 1.0) \times 10^{13}$	40	1.3×10^{12}

[a] Estimated error of 20% in the reproducibility of the measurement.

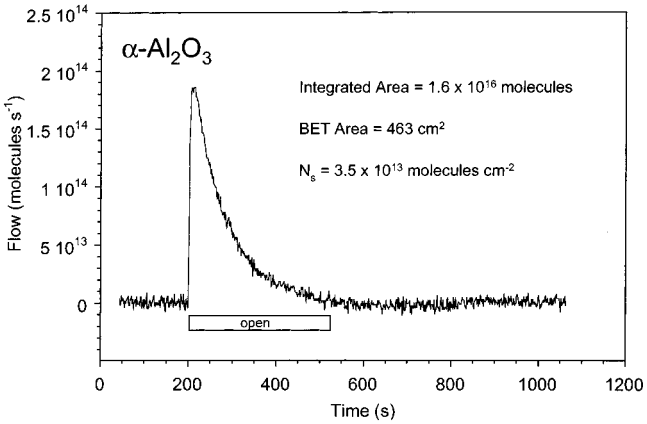

Figure 8. Total uptake measurement for a 3.3 mg sample of α-Al_2O_3 ($P = 40\mu$T, $A_s = 5.07$ cm^2, and $A_h = 0.0484$ cm^2). Flow data have been offset and inverted such that the integrated area represents the total number of molecules of HNO_3 adsorbed. The surface coverage is calculated using the BET surface area.

For any given data point on the graphs in Figure 9, $\gamma_{o,t}$ can be calculated from the known mass (and thus BET area) via eq 4. Alternatively, as was done here, random error can be reduced by using the slope of the best linear fit to the $\gamma_{o,obs}$ versus mass data to determine the true uptake coefficient as follows:

$$\gamma_{o,t} = \text{slope } (mg^{-1}) \frac{A_s\ (cm^2)}{S_{BET}\ (cm^2\ mg^{-1})} \qquad (5)$$

Using eq 5 and the measured S_{BET} values from Table 1 with the best-fit slopes, we determined $\gamma_{o,t}$ values and presented them in Table 5. Inspection of Tables 3 and 5 show that the γ_t values determined for MgO using the LMD model are within approximately 25% of those determined using the pore diffusion model.

Effect of Surface Adsorbed Water on the Heterogeneous Reaction of Nitric Acid. Some investigations into the effect of surface water were also performed, as this has been shown to be important in the uptake of nitric acid on $CaCO_3$[24,25] and NaCl.[26,27] It has been demonstrated that even after pumping overnight, solid particles often retain adsorbed water.[26] The reactivity of these comparatively "wet" samples were compared to samples which had been heated ($\sim$40 °C) during the overnight evacuation. The results for CaO and Gobi dust are plotted in

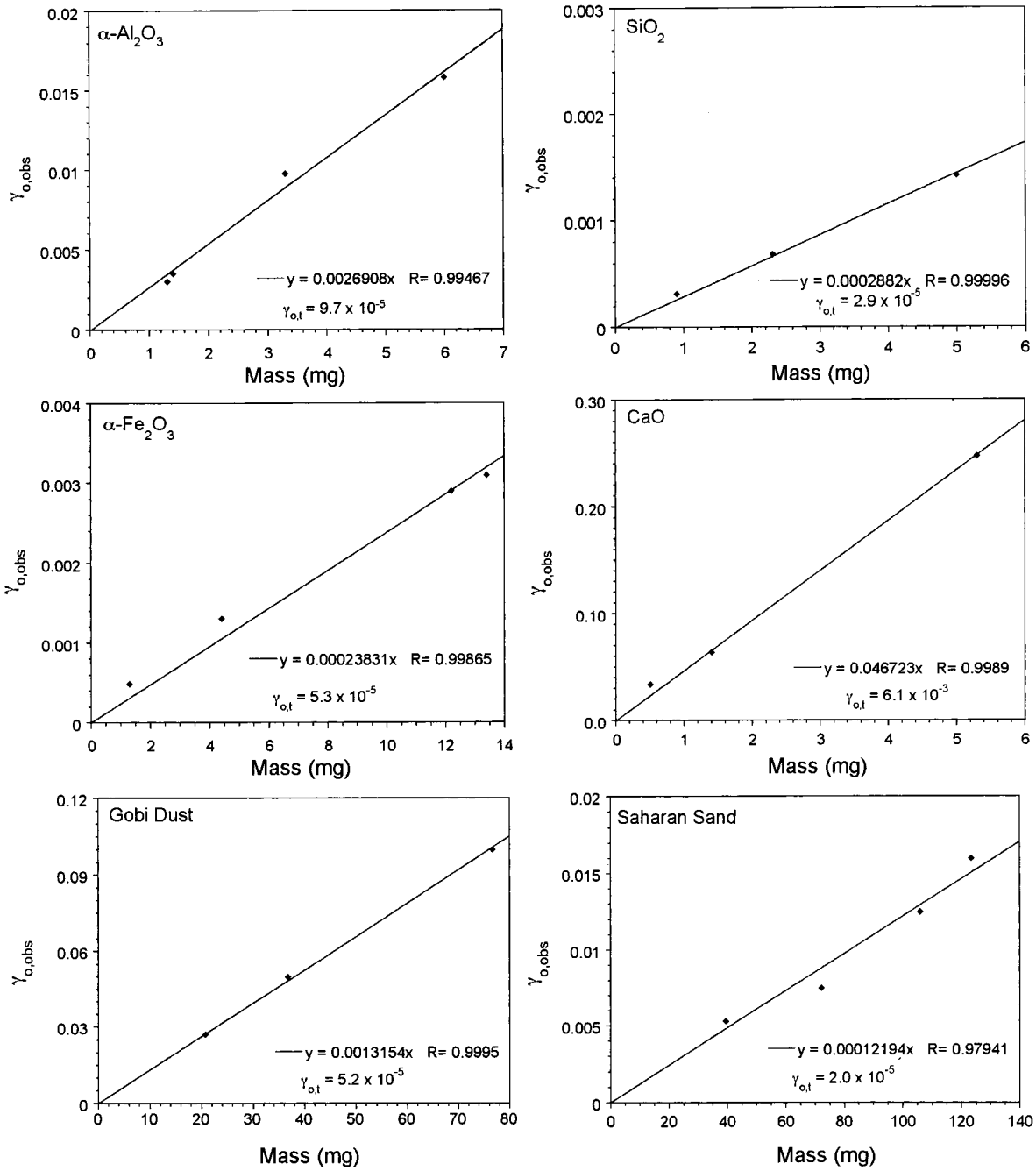

Figure 9. Linear mass dependent regions and data used to determine the true initial uptake coefficients for nitric acid on the oxide particles as well as some authentic dust samples. The true initial uptake coefficients given in each plot is determined from the slope of the lines via eq 5 and the BET surface areas given in Table 1. The parameters used in these experiments are α-Al_2O_3 ($P = 40\mu$T, $A_s = 5.07$ cm^2, and $A_h = 0.0484$ cm^2), SiO_2 ($P = 8\mu$T, $A_s = 5.07$ cm^2, and $A_h = 0.0130$ cm^2), α-Fe_2O_3 ($P = 10\mu$T, $A_s = 5.07$ cm^2, and $A_h = 0.0247$ cm^2), CaO ($P = 40\mu$T, $A_s = 5.07$ cm^2, and $A_h = 0.104$ cm^2), Gobi dust ($P = 40\mu$T, $A_s = 5.07$ cm^2, and $A_h = 0.104$ cm^2), and Saharan sand ($P = 50\mu$T, $A_s = 5.07$ cm^2, and $A_h = 0.104$ cm^2).

TABLE 5: True Initial Uptake Coefficients[a]

sample	$\gamma_{o,obs}$ vs mass slope	$\gamma_{o,t}$
α-Al_2O_3	$2.7(\pm 0.2) \times 10^{-3}$	$9.7(\pm 0.5) \times 10^{-5}$
SiO_2	$2.9(\pm 0.2) \times 10^{-4}$	$2.9(\pm 0.2) \times 10^{-5}$
MgO	$1.1(\pm 0.1) \times 10^{-2}$	$3.7(\pm 0.2) \times 10^{-4}$
α-Fe_2O_3	$2.4(\pm 0.2) \times 10^{-4}$	$5.3(\pm 0.3) \times 10^{-5}$
CaO	$4.7(\pm 0.3) \times 10^{-2}$	$6.1(\pm 0.3) \times 10^{-3}$
Gobi dust	$1.3(\pm 0.1) \times 10^{-3}$	$5.2(\pm 0.3) \times 10^{-5}$
Saharan sand	$1.2(\pm 0.1) \times 10^{-4}$	$2.0(\pm 0.1) \times 10^{-5}$

[a] Calculated using eq 5 and the data from Figures 7 and 9.

Figure 10, where it can be seen that even a small change in the amount of water on the surface can have a significant effect in the uptake coefficient, (a factor of 27 for CaO and 10 for Gobi dust).

Pressure Dependence of the Heterogeneous Reaction of Nitric Acid. A limited number of experiments were done to investigate the pressure dependence of the initial uptake coefficient. The observed initial uptake coefficient for nitric acid on α-Al_2O_3 as a function of sample mass was measured at two different pressures. These data are plotted in Figure 11. It can be seen that the slopes of the lines through the data points are quite different. At a pressure near 40 μTorr, the slope of the line is 12 times greater than that at $P = 100$ μTorr. Thus, a factor of 2.5 increase in pressure results in a factor of 12 decrease in the value of the true initial uptake coefficient. The

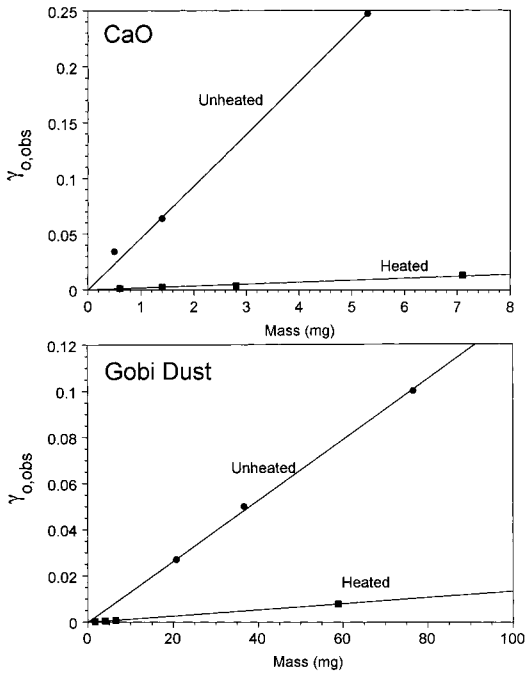

Figure 10. Initial uptake coefficients calculated using eq 1 for unheated and heated samples of both CaO and Gobi dust. The filled circles represent samples which have been evacuated overnight but not heated and thus have a small amount of water adsorbed on the surface. The filled squares depict samples for which much of the water has been removed by heating to 40 °C overnight under vacuum. CaO ($P = 40\mu$T, $A_s = 5.07$ cm^2, and $A_h = 0.104$ cm^2) and Gobi dust ($P = 40\mu$T, $A_s = 5.07$ cm^2, and $A_h = 0.104$ cm^2). For CaO, the slopes of the liners are $y = 0.0467x$ and $y = 0.0017x$ for unheated and heated samples, respectively. When eq 5 and the information in Table 1 were used, the initial uptake coefficients decrease by a factor of 27 and 10 for heated CaO and Gobi dust, respectively, compared to the unheated sample.

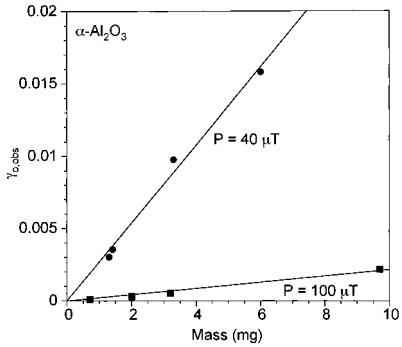

Figure 11. Mass dependent initial uptake coefficients calculated using eq 1 for nitric acid uptake on α-Al_2O_3 at two different pressures, 40 and 100 μTorr. ($A_s = 5.07$ cm^2 and $A_h = 0.0484$ cm^2). The slope of the line at 40 μTorr is $y = 0.0027$ and at 100 μTorr is 0.00022. The true uptake coefficients at 40 and 100 μTorr determined using eq 5 and the BET surface area are $9.7 \pm 0.5 \times 10^{-5}$ and $8.0 \pm 0.4 \times 10^{-6}$, respectively.

pressure dependence can be understood in terms of increased saturation effects that occur at higher pressures. This is discussed in more detail below.

Discussion

Summary of Knudsen Cell Results. The most important point of the models described above is that multiple collisions occur in the underlying layers of a porous sample, causing an amplification of the observed uptake coefficient. This amplification causes the observed uptake coefficient to appear many times larger than its true value. This effect increases the lower limit of uptake coefficients that can be measured for simple systems but significantly complicates the interpretation of the data. Because the net amplification or correction factor for a given system is ultimately dependent on the probe depth, it is useful to consider some of the factors that affect the probe depth and how they impact the systems studied here.

The probe depth is intimately related to the effectiveness factor, η, and is essentially the amount of sample that can be accessed on the time scale of the measurement, which is not to say that particles in the powder deeper than the probe depth are not accessed over the course of the experiment. Though not included in here, total coverage experiments for relatively thick samples have demonstrated that given time the entire sample can be accessed. Presumably, there is a "diffusional front" that moves through the sample. The probe depth is simply the amount of sample the reactant interrogates in the initial stages of the experiment. Its value is dependent upon the relative rates of reaction, γ_t, and diffusion into the underlying layers of the sample. Thus, one of the limitations is that samples must be prepared thin enough to observe a mass dependence. The more reactive the system studied, the more difficult this becomes. Sample preparation technique will certainly impact this effect. For example, without spraying, the smallest amount of sample that can be evenly spread across the entire sample holder for our system is approximately 25 mg for most of the oxides studied. Inspection of Figures 7 and 9 shows that if we were constrained to study samples above this mass, no mass dependence would have been reported for many of the powders studied when in fact there is one. Importantly, a decreased probe depth results in a smaller correction factor, which means that a system for which the linear mass dependence is difficult to experimentally attain may have a $\gamma_{o,t}$ value near that of $\gamma_{o,obs}$.

It is also shown here that the uptake coefficient is a function of coverage (as evidenced by the lower panel of Figures 2−4, γ_{obs} decreases with exposure) and that the true initial uptake coefficient is higher at lower pressures. The pressure dependence of the uptake coefficient reported here for α-Al_2O_3 may be understood in terms of a coverage dependent uptake coefficient. If the impingement rate of the reactant molecules is too high, the incoming gas molecules may start to saturate the limited amount of reactive sites before the first data point is collected; this is especially true when γ is high. If the reacted sites passivate the surface to further reaction, the measured uptake coefficient will be artificially lowered because the measured value for γ will reflect collisions with both active (empty) sites and occupied sites. As will be discussed, this effect will be manifest as a pressure dependence in the observed uptake coefficient. This "limited accommodation" effect can be avoided experimentally by reducing the impingement rate (or pressure), by reducing the data acquisition time, or by a combination of the two. Of course, there is a tradeoff here in that as the pressure is reduced, so is signal intensity, and thus, a compromise must be struck to achieve reasonable signal-to-noise levels. Thus, in reporting true uptake coefficients, we have used the lowest pressure values that we have measured in cases where measurements were made at more than one pressure. A model to account for surface saturation effects is described in more detail below.

Heterogeneous Reactions Mechanism and Kinetic Model for HNO_3 Uptake on Oxide and Mineral Dust Particles. To account for the time, mass, and pressure dependence of the uptake of nitric acid on oxide and mineral dust particles, we developed a kinetic model that can describe both gas diffusion into the powder and saturation effects. From FT-IR studies, it

has been shown that similar to the heterogeneous uptake of HNO_3 on NaCl, the heterogeneous uptake of nitric acid is dissociative and irreversible for the oxide particles investigated here (i.e., HNO_3 (g) $\rightarrow H^+$ (a) + NO_3^- (a)), with the exception of SiO_2, which is molecular (i.e., HNO_3 (g) $\rightarrow$ HNO_3 (a)).[23] Here we will consider the effects of surface coverage and saturation in determining initial uptake coefficients, γ_o, using the simple single-site Langmuir adsorption mechanism found for HNO_3 uptake on NaCl.[28] For this mechanism, the uptake coefficient is a function of coverage and takes the form

$$\gamma = \gamma_o(1 - \theta) \tag{6}$$

where γ is the uptake coefficient, θ is the surface coverage, and γ_o is the uptake coefficient in the limit of zero surface coverage. Assuming a first-order rate process in the gas pressure and the number of available surface sites $(1 - \theta)$, the rate of adsorption can be written as

$$\frac{dN_a}{dt} = k_a p N_s(1 - \theta) \tag{7}$$

where N_a, is the number of adsorbed molecules, k_a is the rate constant for adsorption, p is the pressure of the gas, N_s is the total number of surface sites pressure, and θ is the fractional coverage. If the pressure of the gas is taken to be nearly constant in this flow experiment (i.e., under conditions such that the change in the pressure is small), the rate of the reaction can be analyzed in terms of a pseudo-first-order process with respect to surface sites. With this assumption, and since $N_a = N_s\theta$ and $dN_a = N_s\, d\theta$, eq 7 can be solved, and the solution of the differential expression is

$$\gamma = \gamma_o\, e^{-at} \tag{8}$$

where $a = k_a p$.

The rate of adsorption can also be written as

$$\frac{dN_a}{dt} = \gamma Z = \gamma \frac{p}{\sqrt{(2\pi mkT)}} = \gamma_o(1 - \theta)\frac{p}{\sqrt{(2\pi mkT)}} \tag{9}$$

where Z is the rate of collisions of the gas molecules with the unit surface area, m is the molecular mass of the gas molecule, k is the Boltzmann constant, and T is the absolute temperature. When eq 7 is compared to eq 9, the rate constant becomes

$$k_a = \frac{\gamma_o}{N_s\sqrt{(2\pi mkT)}} \tag{10}$$

Therefore

$$a = k_a p = \frac{\gamma_o p}{N_s\sqrt{(2\pi mkT)}} = 3.154 \times 10^{16}\frac{\gamma_o p}{N_s\sqrt{MT}} \tag{11}$$

where p is in μTorr, N_s is in molecules cm^{-2}, M is the molar mass in g/mol, and T is the absolute temperature in K.

The time-dependent uptake coefficient given in eq 8 can now be put into the rate equations derived for heterogeneous uptake measured with the Knudsen cell technique. The rate of gas flow in a Knudsen cellreactor following time-independent uptake, i.e., when γ is constant, can be written as

$$\frac{dN}{dt} = \text{Flow}_{in} - \text{Flow}_{out} - \text{Flow}_{uptake} = k_{esc}N_o - k_{esc}N - \gamma\frac{A_s}{A_h}k_{esc}N \tag{12}$$

Substituting eq 8 into eq 12, we get

$$\frac{dN}{dt} = k_{esc}N_o - k_{esc}N - k_{esc}N\frac{A_s}{A_h}(\gamma_o e^{-at}) \tag{13}$$

If a mass spectrometer is used to monitor gas flow, this expression can be written in terms of a normalized mass spectral intensity as

$$\frac{dI}{dt} = k_{esc} - k_{esc}I - k_{esc}I\frac{A_s}{A_h}(\gamma_o e^{-at}) \tag{14}$$

For heterogeneous uptake on powdered samples, the uptake coefficient is time-dependent for two reasons. First, as described above, surface saturation is time dependent. Second, gas diffusion into the underlying layers of the sample will also contribute (vide infra).

Since a powdered sample consists of many layers of particles, we have developed a layer-by-layer approach to describe the uptake of a gas by a porous solid. The uptake on each of the individual layers can be described by eq 8, but the gas molecules do not reach all the individual layers at the same time due to the diffusion time through the powder. The first layer is unique because there is no diffusion time in the powder. The uptake can be described for any layer, as follows:

$$\begin{aligned}
&\text{First Layer:} && \gamma_1 = \gamma_0 e^{-at}\\
&\text{Second Layer:} && \gamma_2 = \begin{cases}\gamma_0 e^{-a(t-t_2)}, & \text{if } t \geq t_2\\ 0, & \text{if } t < t_2\end{cases}\\
&\text{Third Layer:} && \gamma_3 = \begin{cases}\gamma_3 e^{-a(t-t_3)}, & \text{if } t \geq t_3\\ 0, & \text{if } t < t_3\end{cases}\\
&n\text{th Layer:} && \gamma_n = \begin{cases}\gamma_0 e^{-a(t-t_n)}, & \text{if } t \geq t_n\\ 0, & \text{if } t < t_n\end{cases}
\end{aligned} \tag{15}$$

where t_2 is the time it takes for gas molecules to diffuse to the second layer, t_3 is the time to get to the third layer, etc. If at any time $t < t_n$, i.e., before the gas molecules can reach the nth layer, there is no uptake on that layer, so the uptake coefficient is set equal to zero. After the gas molecules reach the layer, the uptake process follows eq 8.

The time it takes to get to each layer can be determined from the diffusion time through the powder. The root-mean-square distance l traveled by molecules with effective diffusion constant D_{eff} in time t is given by[29]

$$l = \sqrt{2D_{eff}t} \tag{16}$$

Therefore, the time it takes to diffuse is

$$t = \frac{l^2}{2D_{eff}} \tag{17}$$

For a powder sample with mass m_s and bulk density ρ_b packed in a sample holder with geometric area, A_s, the total thickness, L, is given by

$$L = \frac{m_s}{\rho_b A_s} \tag{18}$$

If the specific BET area of the powder sample is S_{BET}, the total BET area of the powder sample is $m_s S_{BET} = A_{BET}$, the whole powder sample can then be treated as j layers of A_s surfaces stacked one on top of the other with

$$j = \frac{A_{BET}}{A_s} \tag{19}$$

and the distance between two adjacent A_s surfaces is

$$\frac{L}{j} = \frac{1}{S_{BET}\rho_b} \tag{20}$$

The incorporation of saturation and diffusion into eq 14 is then straightforward, and the Knudsen cell equation in terms of the normalized mass spectral intensity becomes

$$\frac{dI}{dt} = k_{esc} - k_{esc}I - k_{esc}I\frac{A_s}{A_h}\left\{\sum_{i=0}^{j}\gamma_o \quad \text{if} \quad \left[t < \frac{\left(\frac{i}{j}L\right)^2}{2D_{eff}}, \quad *0, \quad \text{or} \right.\right.$$
$$\left.\left. *e^{-a[t-((i/j)L)^2/2D_{eff}]}\right]\right\} \tag{21}$$

where

$$i = n - 1 \tag{22}$$

and

$$t_i = \frac{\left(\frac{i}{j}L\right)^2}{2D_{eff}} \tag{23}$$

The "if" clause in eq 21 can be easily implemented in many mathematical packages available today (such as MATHCAD). Equation 21 can be used to model the experimental observations such as the mass and time dependence of the observed uptake. In this equation, the initial uptake coefficient, γ_o, and the effective diffusion constant, D_{eff}, are fitting parameters. Most other parameters in the equation are experimental parameters (pressure, k_{esc}, mass, ρ, A_s, A_{BET}, and mass). The number of surface sites (N_s) can be determined from the experimental data.

Since there is actually a decrease in the gas pressure in the Knudsen cell when molecules adsorb on the powder, we can modify the a term defined in eq 11 to include the pressure change, where I is the normalized mass spectral intensity at any time t. Thus, a now takes the form

$$a = \frac{\gamma_o p(I)}{N_s\sqrt{(2\pi mkT)}} = 3.154 \times 10^{16}\frac{\gamma_o p(I)}{N_s\sqrt{MT}} \tag{24}$$

We have applied this model to the uptake of HNO_3 on α-Al_2O_3. Before comparing the model and the experimental data, it is instructive to look at two limiting cases. The first case is when diffusion is slow and the uptake coefficient is large. In this case, as D_{eff} approaches zero then t_i, the time it takes to diffuse to underlying layers, goes to infinity. Thus, the uptake occurs on the top layer only. The second case is for fast diffusion, as expected when the uptake coefficient is small. In this case, as D_{eff} becomes very large, the second term in the exponential goes to zero. The entire bracketed part of eq 21 then reduces to $jA_s\gamma_o e^{-at} = A_{BET}\gamma_o e^{-at}$; thus, all internal layers are simultaneously contributing to the uptake.

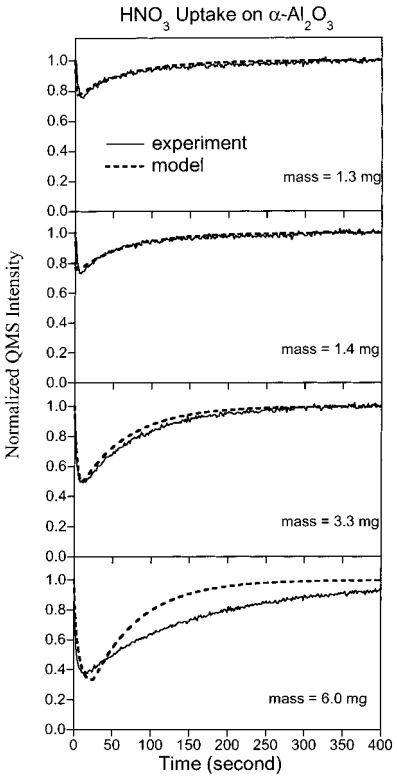

Figure 12. Normalized QMS intensity for heterogeneous uptake of HNO_3 on α-Al_2O_3 compared to the layer-by-layer uptake model. The experimental data are the same as as those shown in Figure 2. The input parameters of the model are given in Table 6. See text for further details.

TABLE 6: Parameters Used in the Layer-by-Layer Uptake Model

parameter	units	value
A_s	cm^2	5.07
A_h	cm^2	0.0484
k_{esc}	s^{-1}	0.020[a]
m	mg	varied[b]
S_{BET}	$cm^2\ mg^{-1}$	140
ρ_b	$mg\ cm^{-3}$	600
p	μTorr	40
N_s	molecules cm^{-2}	3.5×10^{13}
D_{eff}	$cm^2\ s^{-1}$	8.0×10^{-8}
γ_o		6.0×10^{-3}

[a] Determined using the nitric acid exponential decay curve- see text for further detail. [b] Given in Figure 12.

Computer simulations of the model for the uptake of HNO_3 on α-Al_2O_3 as a function of sample mass are presented in Figure 12 and compared to the experimental curves determined for each mass. The experimental and fitting parameters used in the model are given in Table 6. The escape constant, k_{esc}, was determined by flowing HNO_3 through the Knudsen cell until a steady state flow was obtained and then abruptly shutting off the flow of HNO_3. The slope of a plot of the natural log of the HNO_3 mass spectral intensity versus time was used to determine k_{esc}. Since HNO_3 has some affinity for the walls of the Teflon-coated reactor and molecules adsorbed on the walls of the reactor desorb to equilibrate with the lower gas pressure,[30] only the beginning portion of the plot was used to determine the escape constant. In general, HNO_3 does not behave as an ideal gas

because of its nonresidence time with the walls of the reactor. Therefore, the k_{esc} measured for HNO_3 is lower than that measured for ideal gases that follow ideal gas behavior, such as SO_2, by a factor of 5−10.

As seen in Figure 12, the model is found to fit the general shape of the experimental data fairly well. The model shows that the uptake decreases faster for the thinner samples and that the maximum in γ_{obs}, corresponding to a minimum in the normalized QMS intensity, shifts to longer times due to diffusion through the entire powder. The fact that the model does not fit the experimental data exactly, especially at longer times, suggests that the use of a Langmuir model to describe the surface saturation may be an oversimplification. The model also assumes a constant effective diffusion constant. This is probably true in the beginning of the experiment when the surface coverage is very low, but over time, when the surface coverage increases, the effective diffusion constant may change. For the larger masses, wall effects will be more pronounced as the pressure decreases, and re-equilibration of adsorbed nitric acid on the walls of the reactor will become a more substantial effect.

The kinetic model shows that surface saturation can affect the measured value of the uptake coefficient and the uptake measured using the LMD regime is a lower limit to the true uptake coefficient when adsorption and surface saturation occurs on a similar time scale as that of gas diffusion into the underlying layers. The true initial uptake coefficient determined using the layer-by-layer model is a factor of 60 times greater than that determined from the LMD approach for α-Al_2O_3. The layer-by-layer model was applied to nitric acid uptake on the other oxides and found to be in better agreement (factor of 5−10) with the LMD model. For α-Fe_2O_3, SiO_2, Gobi dust, and Saharan sand, this is because the uptake coefficient is sufficiently low such that saturation effects are less important on the time scale of the measurement. For CaO and MgO, although the initial uptake coefficient is higher than that measured for α-Al_2O_3, there are a greater number of surface sites available. An increase in the number of surface sites will also decrease the effects of surface saturation as more sites are available for adsorption.

The pressure also plays a role in surface saturation effects. Using the layer-by-layer model, it is found that there is a decrease in the observed uptake coefficient by a factor of 4 at initial pressure of 100 μTorr compared to 40 μTorr. Although the model predicts the same qualitative trend in the pressure dependence as the experimental data show in Figure 11, it does not quantitatively predict the magnitude. This may be related to the wall effects discussed by Fenter et al., which will be more pronounced at higher nitric acid pressures.[31]

Atmospheric Implications. In a recent report, we have combined laboratory measurements and modeling analysis to quantify the role of heterogeneous reactions of gaseous nitrogen dioxide and nitric acid on oxide and mineral dust particles in tropospheric ozone formation.[16] The impact of heterogeneous reactions of NO_2 and HNO_3 on mineral aerosol in tropospheric ozone formation and on O_3-precursor relationships was assessed using a time-dependent, multiphase chemistry box model. In this model, aerosol interactions with the photochemical oxidant cycles arise through the adsorption of trace species and the gas-to-particle conversions of nitrogen and sulfur species during the aerosol growth and surface heterogeneous reaction processes. Simulations with and without heterogeneous reactions were conducted to evaluate the possible influence of these heterogeneous reactions on ambient levels. In these studies, we have shown that the particles saturate with continued nitric acid exposure and undergo no additional uptake. It is important to take saturation effects into account in atmospheric chemistry models.

Results of the box-model show that values of $\gamma_{HNO_3} > 10^{-5}$ represent a loss mechanism for nitric acid. The heterogeneous loss of HNO_3 results in a large decrease in predicted HNO_3 concentrations (and HNO_3-to-NO_x ratios); however, the effect of a pure heterogeneous loss of nitric acid on ozone and NO_x levels is negligle. This was illustrated in a model run using $\gamma_{HNO_3} = 10^{-3}$, in which no effect was seen on the calculated mixing ratios of either O_3 or NO_x, while that of HNO_3 was reduced by 30%.

It is important to view the data presented in Table 5 as lower limits of the initial uptake cofficient. First, as discussed above, surface saturation effects will lower these values by as much as a factor of 60 in some cases. Second, it is clear from recent experiments that surface-adsorbed water plays an important role in nitric acid uptake on solid particles.[23−27] It is likely that this is so because adsorbed water molecules can provide a medium for the ionic dissociation of nitric acid into nitrate and hydronium ions. As we have demonstrated here, γ_{HNO3} can be greatly enhanced even with small amounts of surface adsorbed water. Under conditions that more closely simulate the atmosphere, i.e., 20−90% RH, it is likely that γ_{HNO_3} would be significantly increased by as much as a factor of 10−100. Thus, the values of all of the initial uptake coefficients for the particle surfaces investigated here will be in the range of 10^{-4} or greater under relevant atmospheric conditions present in the troposphere.

Conclusions

One important conclusion of this work is that, in general, the use of a geometric area in determining the initial uptake coefficient is not justified for nitric acid uptake on oxide and mineral dust powders. Models that take into account gas diffusion into the underlying layers of the powdered sample are needed. A layer-by-layer model was developed to take into account saturation effects as well as gas diffusion into the powder. The layer-by-layer model shows that the LMD and pore-diffusion models give a lower limit to γ_B. It was also shown that even small amounts of surface adsorbed water can greatly enhance reactivity. Thus, the uptake coefficients for nitric acid in the presence of atmospherically relevant water vapor pressures should be even higher. On the basis of a recent box-model study, it is determined that the uptake on mineral dust particles under conditions of 20−50% RH will be sufficiently large to have an impact on nitric acid concentrations in the troposphere. This study also shows that measuring heterogeneous reaction kinetics on powdered samples is complicated because of the many factors that need to be considered and that affect the experimental results.

Acknowledgment. The authors gratefully acknowledge the National Science Foundation (Grant CHE-9988434) and the Department of Energy (DE-FG02-98ER 62580) as well as the Camille and Henry Dreyfus Postdoctoral Program in Environmental Chemistry for support of this research.

References and Notes

(1) Schurath, U.; Naumann, K.-H. *Pure Appl. Chem.* **1998**, *70*, 1353.
(2) Dentener, F. J.; Carmichael, G. R.; Zhang, Y.; Lelieveld, J.; Crutzen, P. J. *J. Geophys. Res.* **1996**, *101*, 22869.
(3) Zhang. Y., Ph.D. Dissertation, The University of Iowa, Iowa City, IA, 1994.
(4) Phadnis, M.; Carmichael, G. R. *J. Atmos. Chem*., in press.
(5) Sheehy, D. P. *Ambio* **1992**, *21*, 303.

(6) Russell, A. G.; Winner, D. A.; Harley, R. A.; McCue, K. F.; Cass, G. R. *Environ. Sci. Technol*. **1992**, *27*, 2772.

(7) Adams, P. J.; Seinfeld, J. H.; Koch, D. M. *J. Geophys. Res*. **1999**, *104*, 13791.

(8) Liu, S. C.; Trainer, M.; Carroll, M. A.; Hubler, G.; Montzka, D. D.; Norton, R. B.; Ridley, B. A.; Walega, G. G.; Atlas, E. L.; Heikes, B. G.; Huebert, B. J.; Warren, W. *J. Geophys. Res*. **1992**, *97*, 10463.

(9) Chatfield, R. B. *Geophys. Res. Lett.* **1994**, *21*, 2705.

(10) Singh, H. B.; Herlth, D.; Kolyer, R.; Salas, L.; Bradshaw, J. D.; Sandholm, S. T.; Davis, D. D.; Crawford, J.; Kondo, Y.; Koike, M.; Talbot, R.; Gregory, G. L.; Sachse, G. W.; Browell, E.; Blake, D. R.; Rowland, F. S.; Newell, R.; Merrill, J.; Heikes, B.; Liu, S. C.; Crutzen, P. J.; Kanakidou, M. *J. Geophys. Res., [Atmos.]* **1996**, *101*, 1793−1808.

(11) Fenter, F. F.; Caloz, F.and Rossi, M. J. *J. Phys. Chem.* **1996**, *100*, 1008.

(12) Keyser, L. F.; Leu, M.-T.; Moore, S. B. *J. Phys. Chem.* **1993**, *97*, 2800.

(13) Keyser, L. F.; Moore, S. B.; Leu, M.-T. *J. Phys. Chem.* **1991**, *95*, 5496.

(14) Aris, R. *The Mathematical Theory of Diffusion and Resaction in Permeable Catalysts*; Clarendon Press: Oxford, 1975; Vol. I.

(15) Underwood, G. M.; Li, P.; Usher, C. R.; Grassian, V. H. *J. Phys. Chem*. **2000**, *104* (4), 819.

(16) Underwood, G. M.; Song, C. H.; Phadnis, M.; Carmichael; G. C.; Grassian V. H. *J. Geophys. Res., [Atmos.]*, in press.

(17) Golden, D. M.; Spokes, G. N.; Benson, S. W. *Angew Chem., Int. Ed. Engl.* **1973**, *12*, 534.

(18) Underwood, G. M.; Miller, T. M.; Grassian, V. H. *J. Phys. Chem. A* **1999**, *103*, 6184.

(19) Golden, D. M.; Manion, J. A. *Advances in Chemical Kinetics and Dynamics* Vol. 1; JAI Press: Greenwich, CT, 1992; pp 187−276.

(20) In this context, the term uptake coefficient refers to the net loss to the sample, which may include both adsorption and reaction on the surface. Though the latter is more formally termed a reaction probability, no such distinction is made here, and the uptake coefficient is used throughout the text.

(21) Dushman, S. *Scientific Foundations of Vacuum Technique*, 2nd ed.; Wiley: New York, 1962.

(22) There is a typographical error in this equation in ref 15 that has been corrected here.

(23) Goodman, A. L.; Bernard, E. B.; Grassian, V. H. *J. Phys. Chem. A*, in press.

(24) Fenter, F. F.; Caloz, F.; Rossi, M. *Atmos. Environ.* **1995**, *29*, 3365.

(25) Goodman, A. L.; Underwood, G. M. *J. Geophy. Res., [Atmos.]* **2000**, *104*, 29, 053.

(26) Beichert, P.; Finlayson-Pitts, B. J. *J. Phys. Chem.* **1996**, *100*, 15218.

(27) Davis, J. A.; Cox, R. A. *J. Phys. Chem. A* **1998**, *102*, 7631.

(28) Ghosal, S.; Hemminger, J. C. *J. Phys. Chem. A* **1999**, *103*, 4777.

(29) Atkins, P. *Physical Chemistry*, 6th ed.; W. H. Freeman and Company: New York, 1998; p754.

(30) For large $\gamma > 10^{-3}$, a normalization factor of $(1 - \gamma)^n$ needs to be included to ensure that the calculated observed uptake coefficient never exceeds a value of 1.

(31) Fenter, F. F.; Caloz, F.; Rossi, M. *J. Phys. Chem.* **1994**, *98*, 9801.